Journal of Materials Chemistry B

Accepted Manuscript

ROYAL SOCIETY OF CHEMISTRY

www.rsc.org/materialsB

Journal of Materials Chemistry B

PAPER

Synthesis and structure of iron- and strontium-substituted octacalcium phosphate: effects of ionic charge and radius

Received 00th January 20xx,
Accepted 00th January 20xx

DOI: 10.1039/x0xx00000x

www.rsc.org/MaterialsB

Haishan Shi,[a, b] Fupo He[d] and Jiandong Ye*[a, b, c]

Octacalcium phosphate (OCP) has received intensive research focus as a main component of bone substitute material due to its highly osteoconductive and biodegradable characteristics. In this work, OCP was synthesized using chemical precipitation methods. Biologically relevant iron ions (Fe^{3+}) and strontium ions (Sr^{2+}) which have different ionic charges and radii were successfully introduced into OCP crystal structure, and their effects on the formation, phase components and structure of OCPs were investigated. The incorporation of Fe^{3+} and Sr^{2+} led to lattice expansion of OCP. Both ionic substitutions had slight effects on the morphology and microstructure of typical plate-like OCP crystals. Particularly, nanosized particles containing rich Fe were deposited on the surface of plate-like Fe^{3+}-substituted OCP crystals, which confirmed the influence of iron substitution on the corresponding crystal surface nature. This work highlights the different replacements of complex Ca sites by Fe and Sr in the apatite layers and hydrated layers of OCP crystal structure, which gives more possible accounts for foreign trivalent and divalent cations.

Introduction

In recent years, octacalcium phosphate (OCP) has drawn growing attention as a main component of synthetic bone substitute materials [1-4]. OCP has been suggested to be one of precursors of biogenic apatite as a transitive phase possibly involved in the first stage of mineralization in bone and dental tissues, although bone mineral is a highly doped calcium deficient apatite which is different from hydroxyapatite (HA) and OCP [5-8]. OCP is metastable with tendency of conversion to HA with similar structure, which is spontaneous and irreversible at physiological pH and temperature. OCP offers a fascinating alternative as a transient intermediate to the biogenic apatite for bone regeneration [9-11].

OCP crystals are composed of apatite layers and hydrated layers [12,13]. Similar to HA, the structural properties of OCP crystals can be changed by many methods, e.g. metal ion substitution, etc [14-16]., to control their biocompatibility. However, the existence of eight calcium sites in the crystal structure of OCP crystals brings more possibilities of complex ionic substitution [17]. Most studies on substitution of impurity cations into OCP crystal structure have been dedicated to the localization of divalent cations, such as Sr^{2+}, Mg^{2+} and Zn^{2+} [15,16,18]. Few studies have focused on the trivalent cations, such as Fe^{3+}, Cr^{3+} and Al^{3+} [19]. Furthermore, the comparative studies of effects of trivalent cations and divalent cations on the formation, phase components and structure of OCP crystals have not been carried out.

The differences between trivalent and divalent cations are mainly the ionic charge and radius. In this work, Fe^{3+} and Sr^{2+}, which were selected as the model trivalent and divalent cations, were introduced into the OCP crystal structure because of their good biological efficacy. Fe is one of the biologically essential trace elements for the survival of human beings, which exists especially in bones and teeth [20]. Fe is also important in the cellular metabolism of all eukaryotic cells, representing a fundamental requirement for the survival and proliferation of cells [21]. Sr is present in the mineral phase of natural bone, balancing bone formation and resorption processes in vivo [22-24]. In addition, Sr and its incorporation into calcium phosphates are of high interest, due to the growing evidences of positive results in the clinical studies [25-27]. Ionic radii of Fe^{3+}, Sr^{2+} and Ca^{2+} are 0.65, 1.20 and 0.99 Å, respectively [28]. The replacements of Ca^{2+} by Fe^{3+} and Sr^{2+} in the HA structure have been studied with different impacts on crystal structure and biomedical of HA, respectively [29-34]. OCP, one of the most important precursors of HA, has more complex crystal structure for the substitution of Fe^{3+} and Sr^{2+} which differ in ionic charge and radius. In this work, Fe^{3+} and Sr^{2+} were incorporated into OCP crystal structure. The effects of trivalent and divalent cations on the formation, phase components and structure of OCP crystals were investigated.

[a] School of Materials Science and Engineering, South China University of Technology, Guangzhou 510640, China. *E-mail: jdye@scut.edu.cn; Tel: +86 020 22236286.
[b] National Engineering Research Center for Tissue Restoration and Reconstruction, South China University of Technology, Guangzhou 510006, China.
[c] Key Laboratory of Biomedical Engineering of Guangdong Province，South China University of Technology, Guangzhou 510641, China.
[d] School of Electromechanical Engineering, Guangdong University of Technology, Guangzhou 510006, China

† Electronic Supplementary Information (ESI) available: [Additional experimental data of the synthesized OCP samples including used chemical reactants, XPS survey spectra, refined results and quantitative surface composition analysis, as well as the initial product of OCP]. See DOI: 10.1039/x0xx00000x

Experimental

Synthesis procedure

OCP samples were prepared using homogeneous precipitation method, and the elemental compositions of used reactants are summarized in **Tab.S1**. In brief, a solution containing 40 mM calcium acetate ($Ca(CH_3COO)_2$) was mixed with a solution containing 30 mM ammonium dihydrogen phosphate ($NH_4H_2PO_4$) and 100 mM carbamide ($CO(NH_2)_2$) by smoothly stirring at 25°C for 5 min, then vigorously stirred at 90°C for 2 h. The ivory-white precipitate was obtained by centrifugation, then washed with deionized water thrice, and air-dried for 24 h at 60°C. Fe- and Sr- substituted OCPs were prepared using same method in the presence of Fe^{3+} and Sr^{2+}, respectively. Ferric nitrate ($Fe(NO_3)_3{\cdot}9H_2O$) and strontium acetate ($Sr(CH_3COO)_2{\cdot}1/2H_2O$) were used together with calcium acetate, respectively, to prepare the solutions with Fe^{3+} or Sr^{2+} concentration of 5 mol.%. The obtained powder samples containing Fe^{3+} and Sr^{2+} were labelled as Fe-OCP and Sr-OCP, respectively. All the used chemicals were analytical reagent and purchased from Sinopharm Chemical Regent Co., Ltd (China). Dynamic pH value of mixed solution during the chemical reaction at 90°C was measured by pH meter (Sartorius, Germany), and the data were recorded every five minutes.

Characterization

Phases of the obtained samples were identified by X-ray diffraction (XRD; X'Pert PRO, PANalytical, the Netherlands) with CuKα radiation (λ = 1.5418 Å, 40 kV, 40 mA). Rietveld refinement was performed using the structural model of OCP (ICSD #65347). Fourier-transform infrared spectroscopy (FTIR) analysis was carried out using a spectrometer (Vector 33-MIR, Brukev Optik, German). Raman spectral analysis was performed by Smart Raman Spectrometer (LabRAM Aramis, HORIBA Jobin Yvon, France) using Nd: YAG laser light at 532.8 nm wavelength. Elemental compositions of the samples were quantified by X-ray fluorescence (XRF) spectrometer (AXIOS, PANalytical, the Netherlands).

Surface elementary compositions of the samples were analysed by an X-ray photoelectron spectroscope (XPS; AXIS Ultra DLD, Kratos, UK) with Al Kα radiation ($h\nu$ = 1486.6 eV). Surface morphology of the samples was observed using a field emission scanning electron microscope (FESEM; Nova NanoSEM 430, FEI, USA) at an accelerating voltage of 15 kV. More surface details were analysed by an atomic force microscope (AFM; MFP-3D, Asylum Research, USA) in air using Tapping Mode with cantilever probes (PPP-NCHR, Nanosensors, USA). Microstructure of the samples was examined using a high resolution transmission electron microscope (HRTEM; JEM-2100F, JEOL, Japan).

Results and discussion

Synthesis procedure and reaction mechanism

In this work, we aimed to introduce trivalent and divalent cations, Fe^{3+} and Sr^{2+}, into OCP crystal structure using homogeneous coprecipitation method. Urea is commonly used as a precipitating agent through hydrolysis to regulate the pH value of reaction system [35]. Variation curves of pH value of hot reaction solutions are given in **Fig.1**. The precipitation processes could be divided into three stages accordingly. At the initial stage, rapid precipitation of brushite (DCPD, $CaHPO_4{\cdot}2H_2O$, JCPDS PDF#09-0077, see **Fig.S**1) resulted in the decrease of pH value. Meanwhile, urea decomposed to carbon dioxide and aqueous ammonia, ionizing new OH^- ions to neutralize H^+ ions in the solution. Subsequently, the precipitated DCPD and Ca^{2+} as well as HPO_4^{2-} gradually reached a chemical equilibrium. PO_4^{3-} began to form with the hydrolysis of urea, meanwhile, OCP appeared. The OH^- contributed by urea could stabilize the newly formed OCP crystals, and pH value slowly increased at a certain speed. The synthesis procedure would involve the chemical reactions as follows:

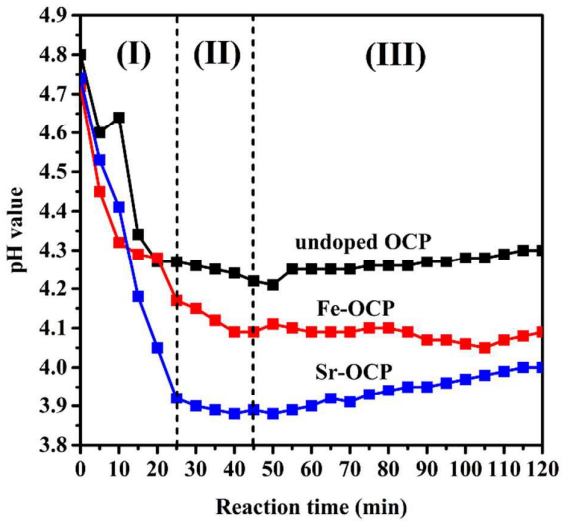

Fig.1 The pH value variation curves of the solutions with reaction time during synthesis.

$$H_2PO^-_{4(aq)} \leftrightarrow HPO^{2-}_{4(aq)} + H^+_{(aq)} \quad (1)$$

$$Ca^{2+}_{(aq)} + HPO^{2-}_{4(aq)} + 2H_2O \leftrightarrow CaHPO_4 \bullet 2H_2O_{(s)} \quad (2)$$

$$CO(NH_2)_2 + 3H_2O \rightarrow 2NH^+_{4(aq)} + 2OH^-_{(aq)} + CO_{2(g)} \quad (3)$$

$$HPO^{2-}_{4(aq)} + OH^-_{(aq)} \leftrightarrow PO^{3-}_{4(aq)} + H_2O \quad (4)$$

$$8Ca^{2+}_{(aq)} + 2HPO^{2-}_{4(aq)} + 4PO^{3-}_{4(aq)} + 5H_2O \leftrightarrow Ca_8H_2(PO_4)_6 \bullet 5H_2O_{(s)} \quad (5)$$

The pH value variation tendency of the reaction solutions containing Fe^{3+} or Sr^{2+} was similar to that of the solution without dopant, but their pH values were lower than that of the solution without dopant at the same reaction time. It was inferred that Fe^{3+} and Sr^{2+} temporarily combined with hydrolysed OH^- or phosphate ions. The possible reactions were as follows:

$$Fe^{3+}_{(aq)}+3OH^{-}\leftrightarrow Fe(OH)_{3(s)} \quad (6)$$

$$2Fe^{3+}_{(aq)}+3H_2PO^{-}_{4(aq)}\leftrightarrow Fe_2(HPO_4)_{3(s)}+3H^{+}_{(aq)} \quad (7)$$

$$2Fe^{3+}_{(aq)}+3HPO^{2-}_{4(aq)}\leftrightarrow Fe_2(HPO_4)_{3(s)} \quad (8)$$

$$Sr^{2+}_{(aq)}+H_2PO^{-}_{4(aq)}\leftrightarrow SrHPO_{4(s)}+H^{+}_{(aq)} \quad (9)$$

$$Sr^{2+}_{(aq)}+HPO^{2-}_{4(aq)}\leftrightarrow SrHPO_{4(s)} \quad (10)$$

Both the consumption of OH^- and generation of H^+ by temporarily forming $Fe(OH)_3$ and $Fe_2(HPO_4)_3$ could contribute to the lower pH value. Similarly, $SrHPO_4$ probably formed transitorily in the reaction solution. These temporary phases gradually disappeared along with the formation of more thermodynamically stable OCPs. These results demonstrated that the Fe^{3+} and Sr^{2+} were involved in the formation of Fe-OCP and Sr-OCP, respectively.

Phase components

XRD patterns of undoped OCP, Fe-OCP and Sr-OCP are shown in **Fig.2a**. All the samples were composed of exclusive calcium hydrogen phosphate hydrate ($Ca_8H_2(PO_4)_6{\cdot}5H_2O$, JCPDS PDF#26-1056). Main characteristic peaks of Fe-OCP and Sr-OCP around 4.7°, 31.7° and 33.5° shifted left when compared to those of undoped OCP, indicating the crystal lattice distortion and bigger interplanar spacings. According to the Bragg Formula, $2d\sin\vartheta = n\lambda$, the decrease of diffraction angle of crystal face is resulted from the increase in interplanar crystal spacing, corresponding to the lattice expansion. The calculated interplanar crystal spacings at (100) and (700) for Fe-OCP and Sr-OCP were both larger than those of undoped OCP (see **Tab.S2**).

Refined results by Rietveld method also revealed the larger lattice parameters of *a*- and *c*- axis as well as unit cell volume of Fe-OCP and Sr-OCP crystals, compared to those of undoped OCP crystals (see **Tab.1**). Elemental molar ratios of these samples are summarized in **Tab.2**. The Fe/(Ca+Fe) molar ratio of Fe-OCP crystals, 4.81%, was slightly lower but very close to its expected value (5%). Comparatively, the experimental value of Sr substitution, 3.08%, was relatively lower than the theoretical datum. The measured molar ratios of Ca/P, (Ca+Fe)/P and (Ca+Sr)/P of corresponding samples were all close to that of the stoichiometric OCP. XRD and XRF results confirmed the successful incorporation of Fe^{3+} or Sr^{2+} into OCP crystals. Substitution of Fe^{3+} and Sr^{2+} did not alter the phase components of characteristic OCP, but led to corresponding lattice distortion.

Journal of Materials Chemistry B

PAPER

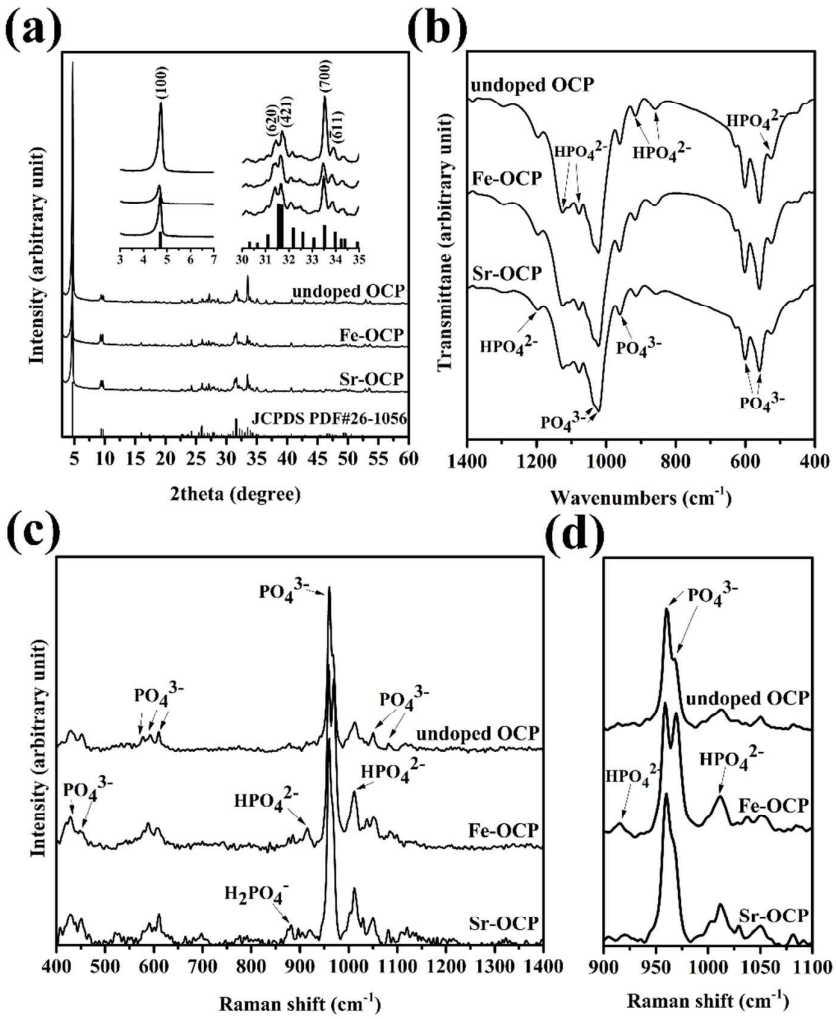

Fig.2 XRD patterns (a) FTIR spectra (b) and Raman spectra (c, d) of undoped OCP, Fe-OCP and Sr-OCP (d is the partial enlargement of c).

Tab.1 Lattice parameters of undoped OCP, Fe-OCP and Sr-OCP crystals.

Sample	*a* (Å)	*b* (Å)	*c* (Å)	*α* (º)	*β* (º)	*γ* (º)	Volume (Å^3)	Rp factor
PDF#26-1056	9.529(0)	18.994(0)	6.855(0)	92.330(0)	90.130(0)	79.930(0)	1220.5(7)	-
undoped OCP	9.397(1)	19.077(3)	6.794(6)	93.384(4)	90.786(0)	80.088(3)	1197.8(0)	4.77%
Fe-OCP	9.544(5)	19.040(9)	6.856(5)	92.517(5)	90.162(0)	79.796(2)	1225.1(6)	4.68%
Sr-OCP	9.567(0)	19.050(1)	6.862(1)	92.611(7)	90.228(4)	79.733(9)	1229.3(3)	3.81%

Journal of Materials Chemistry B

PAPER

Tab.2 Expected and measured elemental molar ratio of undoped OCP, Fe-OCP and Sr-OCP.

Sample	(Ca+M)/P molar ratio*		M/(Ca+M) molar ratio (%)	
	Expected value	Measured value	Expected value	Measured value
undoped OCP	1.33	1.36	-	-
Fe-OCP	1.33	1.37	5.00	4.81
Sr-OCP	1.33	1.35	5.00	3.08

* M stands for Fe or Sr.

FTIR spectra of these samples are shown in **Fig.2b**. Absorption bands at 526, 860, 915 and 1195 cm^{-1} were attributed to the characteristic absorption of HPO_4^{2-}. Two sharp adsorption bands of PO_4^{3-} at 560 cm^{-1} and 602 cm^{-1} were ascribed to crystalline calcium phosphate. These main vibration peaks of phosphate groups were typical of the OCP structure [36,37]. Little difference of these vibration peaks was detected among these samples. Note that no CO_3^{2-} vibration bands can be observed in the spectra, indicating that carbonate was not incorporated into the crystal lattice during the reaction process. More details of phase composition were confirmed by Raman spectra, as shown in **Fig.2c, d**. In all samples, almost all bands corresponding to OCP were presented as in clear support of XRD and FTIR results. The sharp shoulder bands at 960 and 970 cm^{-1} (assigned from P-O vibration) were associated with PO_4^{3-} group in the apatite layer of OCP crystals [37]. Split of the shoulder bands of Fe-OCP crystals at 960 and 970 cm^{-1}, which was referred as Davydov splitting (or called factor-group-splitting), should be due to the presence of more than one (interacting) equivalent molecular entity in the unit cell [38]. In general, at the molecular level, the differences in the mineral ionic environments induced by the ionic substitution could lead to the disruptions of crystal periodicity, as well as alterations of vibrator environments and symmetry. Herein, the split bands should be due to the symmetry change, which could be assigned to two different environments (vacant sites or divalent ions) of the phosphate groups, such as P-O and P-OH groups [39]. It was indicated the charge balance induced by the ferric incorporation, had resulted in the deficiency or promotion of phosphate groups [40]. Compared to the Fe-OCP, the split bands were not detected for the Sr substitution, which should be due to the less complex structure with the coordination environments of apatite layers. The bands at 915 and 1011 cm^{-1} were associated with HPO_4^{2}- group in the hydrated layer of OCP crystals [37]. The intensity of the bands of Fe-OCP and Sr-OCP at 915 and 1011 cm^{-1} were both stronger than that of undoped OCP, which indicated the effects of Fe^{3+} and Sr^{2+} on the hydrated layers of OCP crystal structure. It also confirmed the transition of phosphate groups, especially in the Fe-OCP crystal structure.

XPS survey spectra of these samples are shown in **Fig.S2**. The deconvoluted high-resolution XPS spectra are given in **Fig.3**. Fe and Sr were detected for Fe-OCP and Sr-OCP, respectively. The substitution of Fe^{3+} or Sr^{2+} into OCP hardly alters the main elements species and groups of thin outer surface layers, according to the similar elemental chemical states and binding energy of undoped OCP, Fe-OCP and Sr-OCP. The deconvoluted peaks of Ca2p, P2p and O1s at 347.2, 132.9 and 530.8 eV were attributed to typical OCP crystals (NIST XPS Database). The high spin Fe^{3+} of Fe-OCP was described by a triplet at 711.3, 713.5, 717.2 eV and one satellite peaks at 721.5 eV, respectively. The Fe2p signals were probably due to the existence of FeOOH or Fe(OH)O in the surface layers. Enrichment of Fe had been detected in the surface layer with Fe/(Ca+Fe) molar ratio being 11.792%, compared to Sr/(Ca+Sr) of 0.897% (**Tab.S3**). It indicated that fractional Fe must be deposited on the crystal surface, and Sr was mostly located in the interior of OCP crystals.

Journal of Materials Chemistry B

PAPER

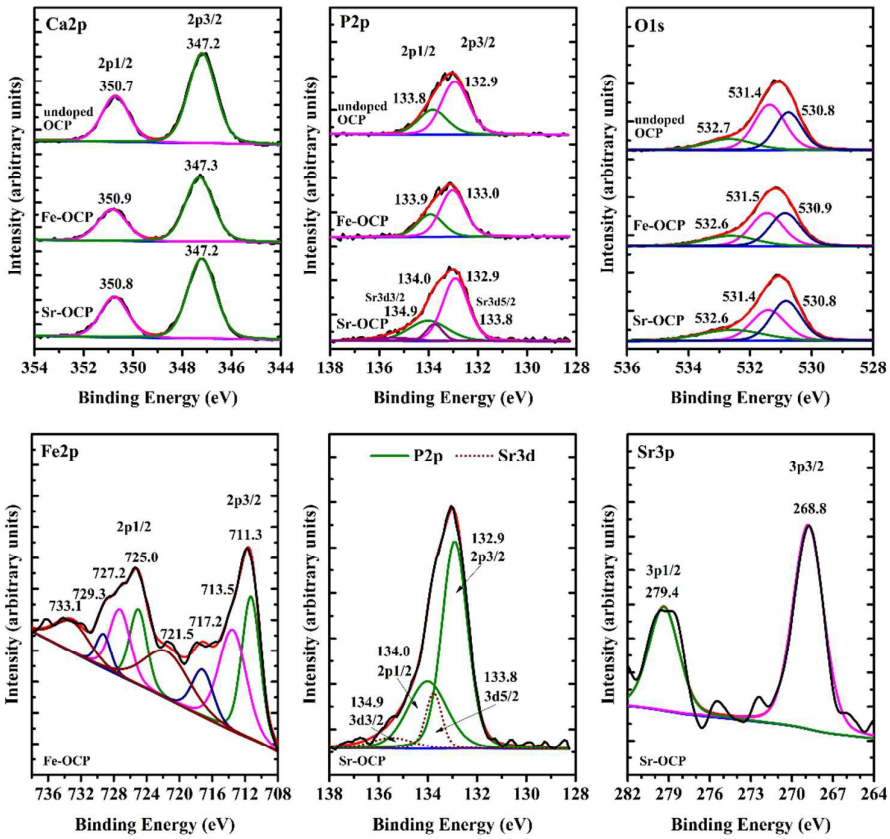

Figure 3 XPS high-resolution results for Ca2p, P2p and O1s of undoped OCP, Fe-OCP and Sr-OCP. Fe2p and Sr3p were detected for Fe-OCP and Sr-OCP, respectively.

Morphology and microstructure

Surface morphology of these samples was observed with SEM and AFM, as shown in **Fig.4**. The crystals of undoped OCP, Fe-OCP and Sr-OCP were all plate-like with lamellar structure, which can be clearly observed from the edges of crystals (**Fig.4d-f**). Little difference of the crystal morphology was detected among these undoped and doped OCPs except the visible surface roughness, as shown in the high-resolution AFM photographs (the inserted enlarged views in **Fig.4d-f**). Sr-OCP crystals had an obviously smoother surface compared to undoped OCP and Fe-OCP crystals. Nanosized particles were found deposited on the Fe-OCP crystal surface (**Fig.4b, e**). These nanosized particles were supposed to form in the synthesis process where ferric ions temporarily combined with hydrolysed OH^- or phosphate ions, which confirmed the relatively high concentration of Fe on the surface of Fe-OCP crystals.

Fig.5 presents the bright field TEM micrographs and HRTEM fringes of undoped OCP, Fe-OCP and Sr-OCP crystals and the corresponding SAED patterns. All the samples displayed well-defined plate-like crystals. Likewise, Fe-OCP crystal surfaces were coated with nanosized particles. The measured interplanar distances corresponding exactly to (002) plane of undoped OCP, Fe-OCP and Sr-OCP crystals were 0.331, 0.340 and 0.335 nm, respectively, which were indicative of the lattice expansion due to ionic substitutions. The results also revealed that these OCP crystals grew much faster along *c*-axis. SAED patterns demonstrated that undoped OCP, Fe-OCP and Sr-OCP were all single-crystal materials with high crystallinity.

Observation of the morphology and microstructure further confirmed the ionic substitution and the deposition of ferric compounds. Both Fe^{3+} and Sr^{2+} were not completely incorporated into OCP crystals along with certain saturated dopant amounts. Furthermore, the residual Fe^{3+} which were not incorporated into Fe-OCP crystals was adsorbed and co-

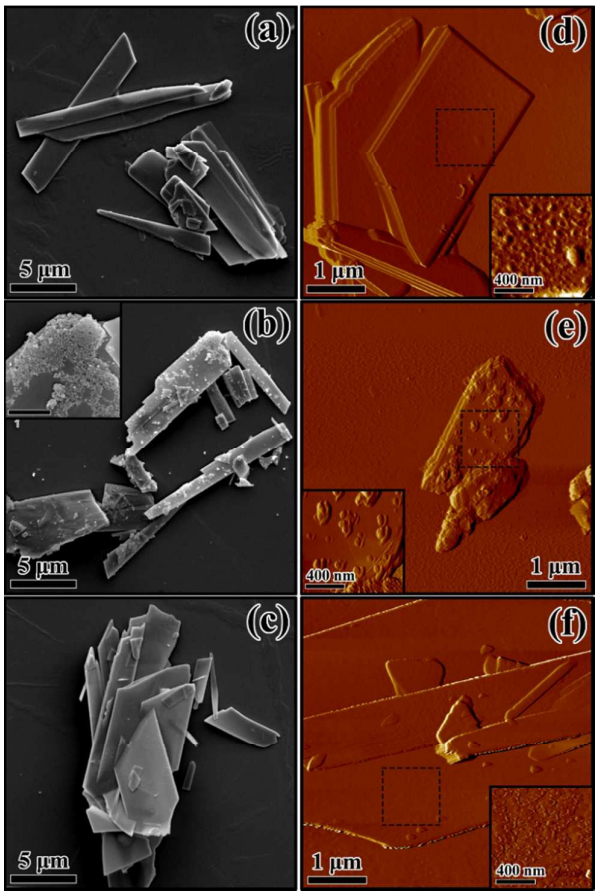

Fig.4 SEM images and AFM images of the microstructure and morphology of undoped OCP (a, d), Fe-OCP (b, e), and Sr-OCP (c, f).

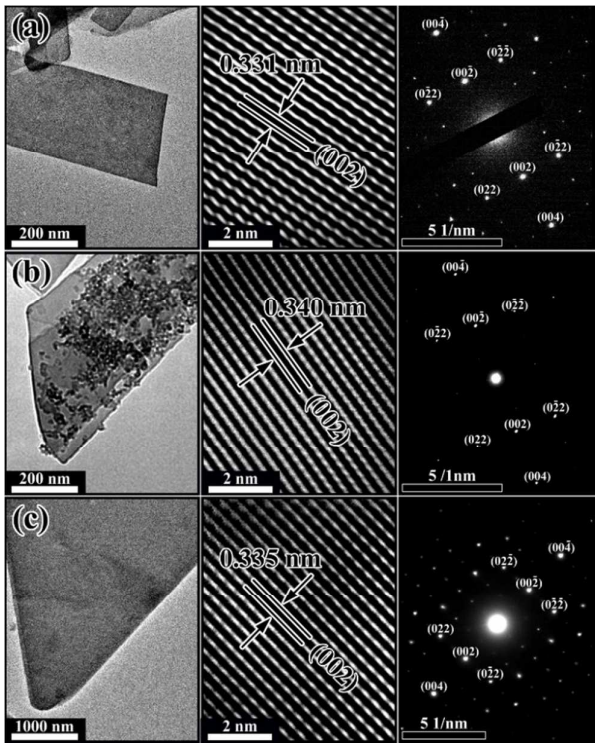

Fig.5 Bright field TEM micrographs, HRTEM fringes and corresponding SAED patterns with [$\bar{1}$00] zone axis of synthetic undoped OCP (a), Fe-OCP (b), and Sr-OCP (c).

deposited on the crystal surface, while the free undoped Sr^{2+} was washed out by the deionized water.

Crystal structure model for ions substitution

In theory, according to the ionic radius, partial one-to-one replacement of Ca^{2+} by Fe^{3+} would result in smaller lattice parameters of *a* and *c*, and the substitution of Ca^{2+} by Sr^{2+} would lead to lager lattice parameters. However, Fe-OCP crystals showed lattice expansion compared to undoped OCP crystals. Hence, to keep the charge balance, Fe was probably incorporated into OCP crystals by partially replacing Ca^{2+} with Fe^{3+} and Fe hydroxo ions ($Fe(OH)_2^+$ or $Fe(OH)^{2+}$), as suggested by M. Wakamura et al [40,41]. In addition, the differences in Raman spectra of HPO_4^{2-} groups between Fe-OCP and undoped OCP presumably resulted from the deficiency of anions (such as PO_4^{3-}) or the promotion of PO_4^{3-} to HPO_4^{2-} /$H_2PO_4^-$ for the charge balance. The deposited nanosized particles containing Fe^{3+} were probably driven by the strong attraction of surface charge and phosphate groups for free cations such as $Fe(OH)^{2+}$ or $Fe(OH)_2^+$ in the solutions. The replacement of Ca^{2+} by Sr^{2+} did not significantly affect the corresponding crystal morphology because of their chemical similarity. Moreover, the incorporation of Sr could stabilize the OCP crystals [42], which led to poor adsorption capacity for other foreign ions along with relatively smooth surface and low amount of Sr^{2+} in the surface layer of Sr-OCP crystals.

Fig.6 displays the unit-cell structure of OCP crystals with the substitution of $Fe(OH)_2^+$, $Fe(OH)^{2+}$ and Sr^{2+} viewed along *c*-axis. The eight kinds of Ca sites in the OCP crystal structure offer quite different stereochemical environments, and this aspect has been focused on understanding the site preference of substitutions. Ca-3 and Ca-4 sites are located in the hydrated layers, and the other Ca sites are in the apatite layers. It was reported that Sr substitutions at the Ca-3, Ca-4 and Ca-8 exhibited much smaller substitution energies than other Ca sites, indicating that OCP can incorporate more Sr^{2+} into these Ca sites of the lattice [43]. In addition, Ca-6 site of OCP is a plausible substitution site to accept small-sized cations, conversely, Ca-3 and Ca-8 sites can essentially accept substitution of large-sized foreign cations [43,44]. Hence, the Sr^{2+} substitution in OCP is energetically most favorable at the Ca-3 and Ca-8 sites. Furthermore, when the [Sr^{2+}] is more than 10^{-4} M, Ca-3 and Ca-8 sites of OCP will be completely substituted by Sr^{2+}. Meanwhile the substitution energy at the Ca-4 decreases, thus Ca-4 site is partially replaced by Sr^{2+} [43].

There are few studies reporting on the substitution of Ca^{2+} by Fe^{3+} in OCP crystals. According to the Fe^{3+} substitution in HA, the Ca (2) site of HA splits into six sites Ca (2a, b, c), Ca (2a, b, c)' and these sites are preferentially occupied by Fe, with essentially equal occupancy. In contrast, the Ca (1) site is found to be essentially not occupied by Fe [45]. The crystal structure of OCP is very similar to that of HA. Ca-1 and Ca-2 in OCP correspond to

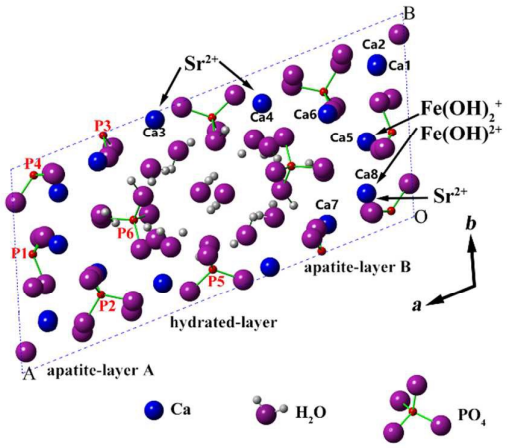

Fig.6 Crystal structure of OCP and corresponding substitutions of Ca^{2+} with $Fe(OH)_2^+$, $Fe(OH)^{2+}$ and Sr^{2+}.

the columnar Ca ions (Ca (1)) in HA, and Ca-5 and Ca-8 in OCP are commensurate with the triangular Ca ions (Ca (2)) in HA. In addition, as above mentioned, Ca-3 and Ca-8 sites are favorable for the large-sized cations. Hence, Ca-8 site of OCP is mostly a substitution site to accept larger ferric hydroxo ions (e.g. $Fe(OH)^{2+}$ or $Fe(OH)_2^+$). Moreover, Mayer *et al*. proposed that Fe^{3+} ions are present in the FeOOH form both in biological and synthetic apatites [46], which has been confirmed by the substitution of ferric hydroxo ions.

In the OCP crystal structure, hydrated layers contain both the hydrogen phosphate groups (P5 and P6) and two of the orthophosphate groups (P2 and P3), while the remaining orthophosphate groups (P1 and P4) are found within apatite layers. The substitution of Fe^{3+} could result in the different coordination environments of P1 and P4, along with the promotion of orthophosphate groups to hydrogen phosphate groups. It has been confirmed by the split shoulder peaks of Raman spectra at 960 and 970 cm^{-1}, as well as the stronger intensity of HPO_4^{2-} group peaks. Sr^{2+} substitution would mainly influence the hydrated layers for its incorporation of Ca-3 and Ca-4 sites. The multiplex kinds of Ca sites are favorable for trivalent and divalent cations with different ionic radii, and simultaneous ionic substitution in the apatite layers and hydrated layers result in a variety of stereochemical environments. Furthermore, the ionic charge of cations (in particular, trivalent cations) would induce the charge imbalance, leading to the lattice distortion along with the vacancy defects or orthophosphate groups promotions.

Conclusions

Fe- and Sr- substituted octacalcium phosphate crystals were synthesized by homogeneous coprecipitation method. The trivalent cations and bivalent cations affected the chemical synthesis process. Synthetic Fe-OCP and Sr-OCP crystals both revealed similar morphology and microstructure to undoped OCP crystals. Lattice expansion of Fe-OCP and Sr-OCP crystals was detected due to the incorporations of ferric hydroxo ions and strontium ions larger than calcium ions. The replacement of Ca sites by Fe mainly affected the apatite layers along with the change of coordination environments, while Sr substitution mostly occurred in the hydrated layers of OCP crystals. The eight kinds of Ca sites and alternate-layered structure of OCP crystals give more possibilities for the site preference of substitutions of trivalent cations and divalent cations, leaving more chances to control the chemical and biomedical properties of calcium phosphates.

Acknowledgements

This research was supported by the National Natural Science Foundation of China under Grant No. 51172074, the National High Technology Research and Development Program of China under Grant No. 2015AA033601, the Science and Technology Program of Guangdong Province of China under Grant No. 2012A061100002, and the Foundation for the Author of the Excellent Doctoral Dissertation of Guangdong Province under Grant No. sybzzxm 201024.

Notes and references

1R. M. Shelton, Y. Liu, P. R. Cooper, U. Gbureck, M. J. German and J. E. Barralet, *Biomaterials*, 2006, **27**, 2874.
2O. Suzuki, S. Kamakura and T. Katagiri, J. Biomed. Mater. Res. B, 2006, **77**, 201.
3Y. Liu, P. R. Cooper, J. E. Barralet and R. M. Shelton, *Biomaterials*, 2007, **28**, 1393.
4S. M. Barinov and V. S. Komlev, *Inorg. Mater. Appl. Res.*, 2010, **1**, 175.
5D. G. Nelson and J. C. Barry, *The Anatomical record*, 1989, **224**, 265.
6B. Wopenka and J. D. Pasteris, *Mat. Sci. Eng. C*, 2005, **25**, 131.
7Y.-H. Tseng, C.-Y. Mou and J. C. C. Chan, *J. Am. Chem. Soc.*, 2006, **128**, 6909.
8J. Tao, K. C. Battle, H. Pan, E. A. Salter, Y.-C. Chien, A. Wierzbicki and J. J. De Yoreo, *P. Natl. Acad. Sci. USA*, 2015, **112**, 326.
9C. Gobel, P. Simon, J. Buder, H. Tlatlik and R. Kniep, *J. Mater. Chem.*, 2004, **14**, 2225.
10 N. J. Crane, V. Popescu, M. D. Morris, P. Steenhuis and M. A. Ignelzi, Jr., *Bone*, 2006, **39**, 434.
11 O. Suzuki, H. Imaizumi, S. Kamakura and T. Katagiri, *Curr. Med. Chem.*, 2008, **15**, 305.
12 W. E. Brown, J. P. Smith, J. R. Lehr and A. W. Frazier, *Nature* 1962, **196**, 1050.
13 M. Mathew, W. E. Brown, L. W. Schroeder and B. Dickens, *J. Crystallogra. Spectrosc. Res.*, 1988, **18**, 235.
14 S. V. Dorozhkin, *Biomaterials*, 2010, **31**, 1465.
15 X. Yang, L. Zhang, X. Chen, G. Yang, L. Zhang, C. Gao, H. Yang and Z. Gou, *Acta. Biomater.*, 2012, **8**, 1586.
16 E. Boanini, M. Gazzano, K. Rubini and A. Bigi, *Cryst. Growth. Des.*, 2010, **10**, 3612.
17 J. C. Elliott, Structure and chemistry of the apatite and other calcium orthophosphates, ELSEVIER, Amsterdam, 1994.
18 Y. Honda, T. Anada, S. Morimoto, Y. Shiwaku and O. Suzuki, *Cryst. Growth. Des.*, 2011, **11**, 1462.
19 H. E. Lundager Madsen, *J Cryst Growth*, 2008, **310**, 2602.

20 P. Guggenbuhl, R. Filmon, G. Mabilleau, M. F. Basle and D. Chappard, *Metabolism*, 2008, **57**, 903.
21 O. Kakhlon and Z. I. Cabantchik, *Free. Radical. Bio. Med.*, 2002, **33**, 1037.
22 G. M. Blake, M. A. Zivanovic, A. J. McEwan and D. M. Ackery, *Eur. J. Nucl. Med.*, 1986, **12**, 447.
23 J. Rodriguez, N. D. Escudero and P. M. Mandalunis, *Acta odontologica latinoamericana : AOL*, 2012, **25**, 208.
24 A. D. Bakker, B. Zandieh-Doulabi and J. Klein-Nulend, *Bone*, 2013, **53**, 112.
25 P. D. Delmas, Osteoporos. Int., 2005, **16** Suppl 1, S16.
26 M. E. Arlot, Y. Jiang, H. K. Genant, J. Zhao, B. Burt-Pichat, J. P. Roux, P. D. Delmas and P. J. Meunier, *J. Bone. Miner. Res.*, 2008, **23**, 215.
27 E. D. Deeks and S. Dhillon, *Drugs*, 2010, **70**, 733.
28 R. D, Modern ceramic engineering: properties, processing, and use in design., CRC Taylor & Francis., 3rd edn edn., 2005.
29 W. Pon-On, S. Meejoo and I. M. Tang, *Mater. Res. Bull.*, 2008, **43**, 2137.
30 Q. Chang, D. L. Chen, H. Q. Ru, X. Y. Yue, L. Yu and C. P. Zhang, *Biomaterials*, 2010, **31**, 1493.
31 Y. Li, J. Widodo, S. Lim and C. Ooi, *J. Mater. Sci.*, 2012, **47**, 754.
32 S. Panseri, C. Cunha, T. D'Alessandro, M. Sandri, G. Giavaresi, M. Marcacci, C. T. Hung and A. Tampieri, *J. Nanobiotechnol.*, 2012, **10**.
33 M. Iafisco, M. Sandri, S. Panseri, J. M. Delgado-Lopez, J. Gomez-Morales and A. Tampieri, *Chem. Mater.*, 2013, **25**, 2610.
34 W. Pon-On, N. Charoenphandhu, J. Teerapornpuntakit, J. Thongbunchoo, N. Krishnamra and I. M. Tang, *Mater. Chem. Phys.*, 2013, **141**, 850.
35 X. Lu, Y.-b. Wang, J.-x. Wang, S.-x. Qu, J. Weng, R.-l. Xin and Y. Leng, *J. Cryst. Growth.*, 2006, **297**, 396.
36 C. Rey, O. Marsan, C. Combes, C. Drouet, D. Grossin and S. Sarda, *Characterization of Calcium Phosphates Using Vibrational Spectroscopies*, Springer Berlin Heidelberg, 2014.
37 B. O. Fowler, M. Markovic and W. E. Brown, *Chem. Mater.*, 1993, **5**, 1417.
38 C. E. Bonner, C. C. Chess, C. Meegoda, S. Stefanos and G. B. Loutts, *Opt. Mater.*, 2004, **26**, 17.
39 G. Penel, G. Leroy, C. Rey and E. Bres, *Calcified. Tissue. Int.*, 1998, **63**, 475.
40 M. Wakamura, K. Kandori and T. Ishikawa, *Colloid Surface A*, 2000, **164**, 297.
41 K. Kandori, S. Toshima, M. Wakamura, M. Fukusumi and Y. Morisada, *J. Phys. Chem. B*, 2010, **114**, 2399.
42 S. Rokidi and P. G. Koutsoukos, *Chem. Eng. Sci.*, 2012, **77**, 157.
43 K. Matsunaga and H. Murata, *J Phys Chem. B*, 2009, **113**, 3584.
44 K. Matsunaga, J. Chem. Phys., 2008, **128**, 245101.
45 M. Jiang, J. Terra, A. M. Rossi, M. A. Morales, E. M. B. Saitovitch and D. E. Ellis, *Phys. Rev. B*, 2002, **66**, 15.
46 I. Mayer, H. Diab and I. Felner, *J Inorg. Biochem.*, 1992, **45**, 129.
47

Graphical abstract

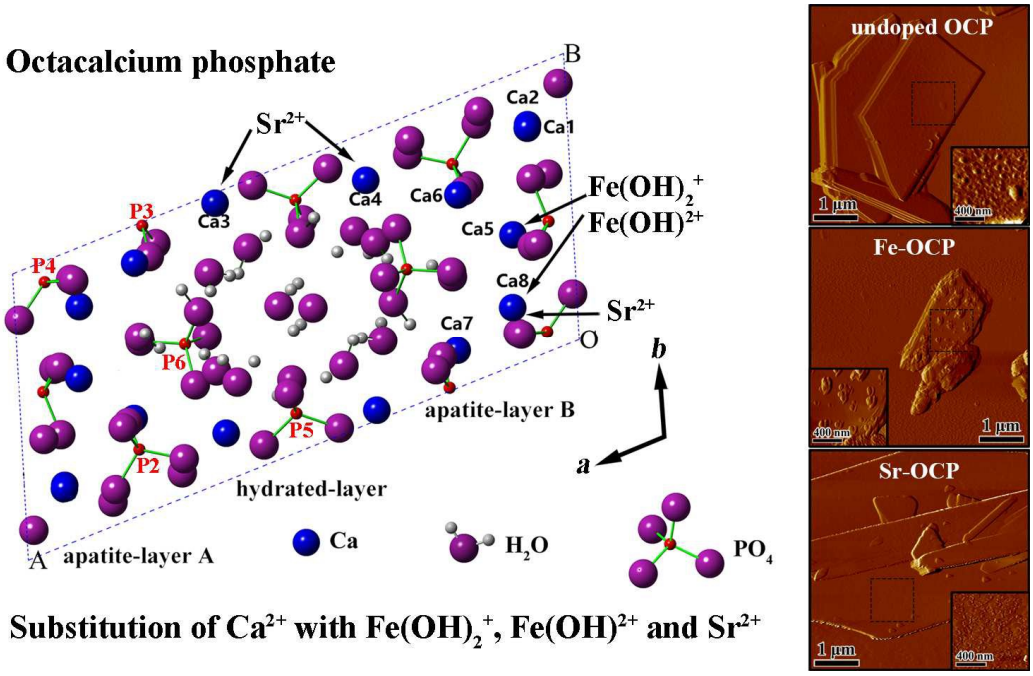

Substitution of Ca^{2+} with $Fe(OH)_2^+$, $Fe(OH)^{2+}$ and Sr^{2+}

Comparative study of Fe^{3+}-/Sr^{2+}- substitution in the apatite and hydrated layers of octacalcium phosphate crystal structure with changed coordination environments.